

Parameterization of subgrid-scale energy injection in oceanic flows

Meelis J. Zidikheri* Jorgen S. Frederiksen†

12 May 2008

Abstract

Dissipative terms are usually employed to parameterize subgrid fluxes of energy and enstrophy in turbulent flows. However, in certain flows, such as oceanic flows, when the dissipation is calculated self-consistently it turns out to be negative and hence numerically unstable. A solution to this problem is offered in this study in the form of a stochastic subgrid-scale parameterization scheme. Using a baroclinic model with typical oceanic parameters, it is shown that the scheme is able to maintain the resolved-scale spectra exceptionally well when the energy injection scale is in the subgrid scales. This work has implications for oceanic circulation modelling, where the deformation (injection) scale is too small to be adequately resolved.

Contents

1	Introduction	2
2	The Baroclinic Model	3
3	Subgrid-scale Parameterizations: Methodology	6
4	Subgrid-scale Parameterizations: Application	7
5	Discussion and Conclusion	11

*Department of Theoretical Physics, Research School of Physical Sciences and Engineering, Australian National University, Canberra, AUSTRALIA. <mailto:meelis.zidikheri@csiro.au>

†CSIRO Marine and Atmospheric Research, Aspendale, Victoria, AUSTRALIA

1 Introduction

Direct Numerical Simulations (DNSs) of turbulent flows require that the smallest scales of motion be resolved due to the non-linear coupling between different scales of motion. Unfortunately, the range of scales excited can be vast for high Reynolds number flows. For example, in the atmosphere and oceans, the range of scales can be $10^7 - 10^{-2}$ m [1]. This presents a formidable computational challenge. A solution to this problem is to perform simulations at manageable resolutions, and to parameterize the interactions with the subgrid scales in some fashion. These simulations are called Large Eddy Simulations (LESs). Practically all climatic simulations with general circulation models of the ocean and atmosphere fall into this category.

Large scale oceanic and atmospheric flows are quasi two-dimensional flows. In the inviscid limit, two-dimensional flows possess two quadratic invariants, namely, energy and enstrophy. The phenomenology of two-dimensional turbulence predicts that enstrophy injected at some intermediate scale is cascaded towards smaller scales (higher wavenumbers) while energy is cascaded towards the large scales (lower wavenumbers). The classical subgrid-scale parameterization scheme employs the so-called eddy viscosity and its variants. In atmospheric and oceanic modelling, this commonly takes the form of a hyperviscosity, which is a very scale-selective damping term that removes enstrophy near the truncation scale.

However, as shown by Leith [2] and Kraichnan [3], there is a problem with this approach when it is used in quasi two-dimensional flows. Because of the dual cascade, the eddy viscosity should actually be negative at the large and intermediate scales. This represents an injection of energy from the subgrid scales. Furthermore, the approaches above have the deficiency of being deterministic. As noted by Herring [4], subgrid-scale motions are inherently chaotic, and must be treated in a stochastic manner. Errors, however small, in estimating the subgrid contributions will grow and eventually contaminate the large scales. This view is consistent with statistical closure theories. In these formulations, it can be shown that the subgrid tendency can be written as a combination of linear deterministic and noise terms, as demonstrated by Frederiksen and Davies for quasi two-dimensional atmospheric flows [5].

In the atmospheric context, deterministic eddy viscosity formulations may appear to be sufficient in many situations, such as in climate studies. In the oceanic context, however, the situation is quite different. Because the oceanic radius of deformation is only about 50 km, the scale of energy injection (due to baroclinic instability) is unresolved in oceanic circulation models. From the barotropic (depth independent) point of view, the subgrid scales act as a source of energy, due to the inverse cascade process of two-dimensional

turbulence, and there is no actual net dissipation. From the stratified (two-layer) turbulence point of view [6], there are two vertical modes: barotropic (vertical average) and baroclinic (vertical shear). The barotropic part of the flow receives energy from the subgrid scales while the baroclinic part of the flow sends energy to the subgrid scales. Hence, a dissipative term might be appropriate for the baroclinic part of flow, but not the barotropic part.

Clearly, if one were to pursue the deterministic eddy viscosity approach consistently in low resolution oceanic flows, then one has to define a negative eddy viscosity. This is, however, numerically unstable. In contrast, within a stochastic formulation, the energy injection occurs via a random forcing term, which is combined with a damping term, leading to a more numerically stable simulation. The methodology that we employ was articulated and used by Frederiksen and Kepert [7] in the context of atmospheric barotropic flows. It is a stochastic method that uses DNS to calculate the statistics of the flow, and is thus easily applicable to a variety of flows. Frederiksen and Kepert showed that the calculated damping parameter (drain eddy dissipation), and the variance of the random forcing (stochastic backscatter) are similar to those calculated from closure theories [5]. In the two-level (baroclinic) case, the scalar parameters are generalized to 2×2 matrices at each wavenumber to account for correlation in the vertical [8].

The outline for the rest of this article is as follows. In Section 2, we introduce the baroclinic model, and run it at high resolution. In Section 3, we discuss the DNS-based stochastic subgrid-scale parameterization method. In Section 4, we apply the subgrid-scale parameterization methodology to the baroclinic model, truncated at a resolution that does not resolve most of the energy injection region. In Section 5, we summarize and discuss the results.

2 The Baroclinic Model

The two-level quasigeostrophic potential vorticity (QGPV) equations equations form the so-called Baroclinic Model. When relaxed towards a mean zonal shear, they generate exponentially growing modes (baroclinic instability) peaked at a wavenumber somewhat larger than the deformation scale, which is around 50 km for the ocean. The spectral form of these equations is

$$\frac{\partial q_{mn}^i}{\partial t} = i \sum_{pq} \sum_{rs} A_{nqs}^{mpr} \zeta_{-pq}^i q_{-rs}^i - D_0^i \zeta_{mn}^i + \kappa \left(\tilde{q}_{mn}^i - q_{mn}^i \right), \quad (1)$$

where $i = 1$ or 2 , m is the zonal wavenumber, and n is the total wavenumber;

$$q_{mn}^i = \zeta_{mn}^i - (-1)^i \frac{F}{n(n+1)} (\zeta_{mn}^1 - \zeta_{mn}^2) \quad (2)$$

is the potential vorticity wave amplitude, which is the field that is stepped forward in time; ζ_{mn}^i is the vorticity; and

$$D_0^i = \alpha_i + \nu_i [n(n+1)]^p + Bi \frac{m}{n(n+1)} \quad (3)$$

is a generalized complex operator that describes both dissipation and the frequency of Rossby waves if $B \neq 0$. On the sphere, $B = 2$; however, for the results presented here we have set $B = 0$ to maintain the vertical symmetry of the flow. \tilde{q}_{mn}^i is the value towards which q_{mn}^i is being relaxed on a timescale given by κ^{-1} ; it is a representation of (Equator-Pole) differential heating effects. The interaction coefficients $A_{nqs}^{mpr} = -\frac{1}{q(q+1)} K_{nqs}^{mpr}$, with K_{nqs}^{mpr} explicitly given by Frederiksen and Kepert [7], describe the non-linear coupling between the streamfunction and vorticity. The non-linear terms are not computed using interaction coefficients as implied in Eq. 1, but the Grid Transform method [9] is used instead. The timestepping is done by the leap-frog method with the introduction of a Modified Euler Backward timestepping scheme after every 96 steps. The Modified Euler Backward scheme is also used for the first timestep. The viscous terms are known to lead to instability of the solutions if implemented by using the standard leap-frog scheme. This is overcome by evaluating the viscous terms using a lagged field; that is, the viscous terms at time t_i are evaluated using the potential vorticity at time t_{i-1} when using the leap-frog method.

In this study, the following parameters have been chosen. The drag, α_i , has been set to a damping time of 20 days for both layers; the hyperviscosity $\nu_i = 1.68 \times 10^8 \text{ m}^4\text{s}^{-1}$ for both layers; the order of the Laplacian operator $p = 2$. The zonal wind is relaxed towards $\tilde{u}_i = \tilde{U}_i \cos\phi$, where ϕ is the latitude, and \tilde{U}_i are the maximum winds (at the equator), implying that only the solid-body-rotation mode with $(m, n) = (0, 1)$ is relaxed; the maximum zonal winds are $\tilde{U}_1 = 0.1875 \text{ ms}^{-1}$ and $\tilde{U}_2 = -0.1875 \text{ ms}^{-1}$; the relaxation time, κ , was 1.16 days. The layer coupling constant, $F = 2.4 \times 10^{-10} \text{ m}^{-2}$, corresponding to a deformation radius of about 50 km. The resolution corresponds to triangular truncation at wavenumber 252 (T252) with 768×384 grid points. The model has been integrated to statistical steady state and then further stepped forward in time for 104 days. With this choice of parameters, and by setting $B = 0$, the kinetic energy is equally distributed across the two layers. Such a flow was considered by Salmon [6], and coined *Equivalent Layers*. The motivation for considering equivalent layers is the high degree of symmetry, which aids understanding and simplifies the presentation of the results.

Fig. 1(a) shows the kinetic and potential energy spectra. An inspection of the kinetic energy spectra reveals a constant slope region, usually associ-

ated with an inertial range, for (m, n) between about 40 to somewhat over 100. The slope of the inertial range is around -2.2, which is steeper than the $-\frac{5}{3} = -1.67$ slope predicted for an inverse energy cascade in QG turbulence. A simple calculation reveals that a deformation scale of 50 km corresponds to a wavenumber of about 120. Hence the energy at wavenumbers substantially smaller than this, including the peak, which is in the range $20 < n < 30$, must be due to an inverse cascade. This view is strengthened by Fig. 1(b), which shows the corresponding spectra in the barotropic-baroclinic (BTBC) formulation where the barotropic vorticity is defined as $\zeta_{mn}^+ = \frac{1}{2}(\zeta_{mn}^1 + \zeta_{mn}^2)$ and the baroclinic vorticity as $\zeta_{mn}^- = \frac{1}{2}(\zeta_{mn}^1 - \zeta_{mn}^2)$. The transient kinetic energy peak is seen to be dominated by barotropic kinetic energy. The baroclinic kinetic energy is much broader, and more significantly, is peaked at around $n = 100$. In the oceanic problem considered here, commonly-used truncations at T126 and below are probably within the inverse cascade region, or within the injection region. Ad-hoc hyperdiffusion schemes are unlikely to be relevant in those regions. The methodology for subgrid-scale parameterizations considered in this study is completely general, however, and should be applicable there.

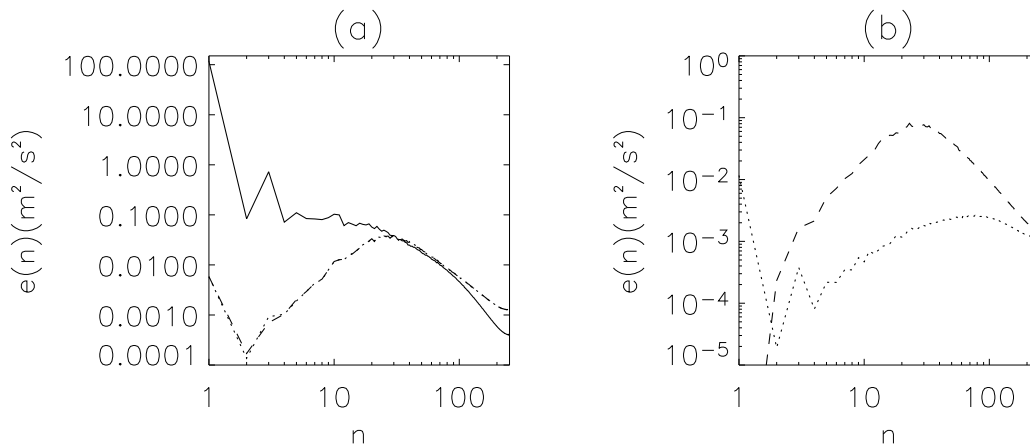


Figure 1: Energy spectra as functions of total wavenumber: (a) potential energy (solid), Level 1 kinetic energy (dashed), and Level 2 kinetic energy (dotted); (b) barotropic kinetic energy (dashed) and baroclinic kinetic energy (dotted).

3 Subgrid-scale Parameterizations: Methodology

It is possible to write the spectral equations of motion of prognostic flow variables, represented by the vector \mathbf{x} , in generic form as follows:

$$\frac{\partial \mathbf{x}(t)}{\partial t} = \left(\frac{\partial \mathbf{x}(t)}{\partial t} \right)_R + \left(\frac{\partial \mathbf{x}(t)}{\partial t} \right)_S. \quad (4)$$

In this study, \mathbf{x} represents the resolved potential vorticity wave amplitudes for the two-level QGPV equations. The vector $\left(\frac{\partial \mathbf{x}(t)}{\partial t} \right)_R$ represents the tendencies of the spectral wave amplitudes involving only resolved-scale amplitudes. The vector $\left(\frac{\partial \mathbf{x}(t)}{\partial t} \right)_S$ represents the tendencies of the spectral wave amplitudes involving subgrid-scale amplitudes. As the latter cannot be explicitly calculated in high Reynolds number simulations, they need to be parameterized in terms of resolved-scale amplitudes. In general, the subgrid tendency has both mean and transient parts:

$$\left(\frac{\partial \mathbf{x}(t)}{\partial t} \right)_S = \bar{\mathbf{f}} + \left(\frac{\partial \hat{\mathbf{x}}(t)}{\partial t} \right)_S, \quad (5)$$

where $\bar{\mathbf{f}}$ and $\left(\frac{\partial \hat{\mathbf{x}}(t)}{\partial t} \right)_S$ are the mean and transient parts, respectively. In this study, the mean part is simply calculated from a high-resolution simulation as the time-average of the subgrid tendency. The transient part is the main focus of this study, and we shall consider both deterministic and stochastic parameterizations. The deterministic scheme is constructed as follows:

$$\left(\frac{\partial \hat{\mathbf{x}}(t)}{\partial t} \right)_S = -\mathbf{D}_n \hat{\mathbf{x}}(t), \quad (6)$$

where \mathbf{D}_n is defined as the net dissipation matrix; $\hat{\mathbf{x}} = \mathbf{x} - \bar{\mathbf{x}}$ is the transient part of \mathbf{x} ; and $\bar{\mathbf{x}}$ is the mean part of \mathbf{x} . Multiplying Eq. 6 by $\hat{\mathbf{x}}^\dagger(t)$ and averaging, we obtain

$$\mathbf{D}_n = - \left[\left\langle \left(\frac{\partial \hat{\mathbf{x}}(t)}{\partial t} \right)_S \hat{\mathbf{x}}^\dagger(t) \right\rangle \right] \left[\langle \hat{\mathbf{x}}(t) \hat{\mathbf{x}}^\dagger(t) \rangle \right]^{-1}. \quad (7)$$

Here, angular brackets denote either ensemble or time averaging; in this study, we shall consider the latter. The stochastic scheme is constructed as follows:

$$\left(\frac{\partial \hat{\mathbf{x}}(t)}{\partial t} \right)_S = -\mathbf{D}_d \hat{\mathbf{x}}(t) + \hat{\mathbf{f}}(t). \quad (8)$$

Here, \mathbf{D}_d is defined as the drain dissipation matrix and $\hat{\mathbf{f}}$ is a random forcing vector. As shown by Frederiksen and Kepert [7], the drain dissipation matrix may be computed by multiplying Eq. 8 by $\hat{\mathbf{x}}^\dagger(t_0)$ (where $t_0 < t$), integrating over the time interval $\tau = t - t_0$ and averaging. Hence,

$$\mathbf{D} = - \left[\int_{t_0}^t ds \left\langle \left(\frac{\partial \hat{\mathbf{x}}(s)}{\partial t} \right)_S \hat{\mathbf{x}}^\dagger(t_0) \right\rangle \right] \left[\int_{t_0}^t ds \langle \hat{\mathbf{x}}(t) \hat{\mathbf{x}}^\dagger(t_0) \rangle \right]^{-1}. \quad (9)$$

The noise covariance matrix

$$\mathbf{F} = \langle \hat{\mathbf{f}}(t) \hat{\mathbf{x}}^\dagger(t) \rangle + \langle \hat{\mathbf{x}}(t) \hat{\mathbf{f}}^\dagger(t) \rangle \quad (10)$$

may be obtained from the Lyapunov equation

$$\left\langle \left(\frac{\partial \hat{\mathbf{x}}(t)}{\partial t} \right)_S \hat{\mathbf{x}}^\dagger(t) \right\rangle + \langle \hat{\mathbf{x}}(t) \left(\frac{\partial \hat{\mathbf{x}}(t)}{\partial t} \right)_S^\dagger \rangle = -\mathbf{D}_d \langle \hat{\mathbf{x}}(t) \hat{\mathbf{x}}^\dagger(t) \rangle - \langle \hat{\mathbf{x}}(t) \hat{\mathbf{x}}^\dagger(t) \rangle \mathbf{D}_d^\dagger + \mathbf{F}(t) \quad (11)$$

after computing \mathbf{D}_d . The forcing, $\hat{\mathbf{f}}(t)$, is assumed to be white noise satisfying

$$\langle \hat{\mathbf{f}}(t) \hat{\mathbf{f}}^\dagger(t') \rangle = \mathbf{F}(t) \delta(t - t'), \quad (12)$$

where $\delta(t - t')$ is the Dirac delta function. It can be shown [8] that $\hat{\mathbf{f}}$ may be computed from

$$\hat{\mathbf{f}} = \frac{1}{\sqrt{2\Delta t}} \mathbf{P} \mathbf{g}, \quad (13)$$

where \mathbf{P} is a unitary matrix whose columns consist of the eigenvectors of \mathbf{F} and

$$\mathbf{g} = \begin{pmatrix} \sqrt{\lambda_1} r_1 \\ \sqrt{\lambda_2} r_2 \end{pmatrix}, \quad (14)$$

where λ_1 and λ_2 are the eigenvalues of \mathbf{F} ; r_1 and r_2 are random numbers with Gaussian distributions. $\frac{1}{\sqrt{2\Delta t}}$ is the finite-difference form of the Dirac delta function with Δt being the timestep.

4 Subgrid-scale Parameterizations: Application

The subgrid tendency is determined from Eq. 4, with the resolved scale tendency, $\left(\frac{\partial q_{mn}^i}{\partial t} \right)_R$, calculated by evaluating Eqs. 1 and 2 using a ‘masked’ field, defined as

$$(\zeta_{mn}^i)_M = \begin{cases} \zeta_{mn}^i & \text{if } m, n < N_*; \\ 0 & \text{otherwise.} \end{cases} \quad (15)$$

Here, N_* is either 31 or 126. The subgrid tendency is calculated at every timestep and stored. Equations 7, 9, and 11 can then be used to calculate the matrix parameters \mathbf{D}_n , \mathbf{D}_d , and \mathbf{F} . We study subgrid-scale parameterizations at T31 using a two-stage procedure. Firstly, an LES is constructed at T126, and then this LES is used to calculate the matrix parameters for the T31 LES. Following Frederiksen and Kepert [7], we take the flow to be horizontally homogeneous; however, in this study we retain the vertically homogeneities. Hence, the matrix parameters, \mathbf{D}_n , \mathbf{D}_d , and \mathbf{F} in Section 3 become 2×2 matrices for each wavenumber, and the vector $\bar{\mathbf{f}}$ becomes two dimensional. The dissipation matrix will in general have eight wavenumber-dependent elements, if we include the real and imaginary parts, and the forcing covariance matrix will have six, bringing the total number of elements to fourteen. The system is simplified somewhat if we work with the barotropic and baroclinic modes defined in Section 2. Then it is easy to show that the matrices \mathbf{D}_d and \mathbf{F} transform into $\mathbf{D}'_d = \mathbf{T}\mathbf{D}_d\mathbf{T}^{-1}$ and $\mathbf{F}' = \mathbf{T}\mathbf{F}\mathbf{T}^\dagger$, where

$$\mathbf{T} = \frac{1}{2} \begin{pmatrix} 1 & 1 \\ \frac{1}{c} & -\frac{1}{c} \end{pmatrix}. \quad (16)$$

Here, $c = 1 + \frac{2F}{n(n+1)}$. Because of the symmetry of the equivalent-layer system, it turns out that \mathbf{D}'_d and \mathbf{F}' have purely real diagonal elements and purely imaginary off-diagonal elements. Hence the total number of elements reduces to just eight, including real and imaginary parts.

The matrix parameters are firstly calculated for $N_* = 126$ using a sampling time of 104 days and $\tau = 1$ day. An LES is then performed at T126, and this is run for 2700 days. The parameters \mathbf{D}'_n , \mathbf{D}'_d , and \mathbf{F}' were calculated from this simulation with $N_* = 31$; they are shown in Fig. 2 after being averaged over the zonal wavenumber m . Note that the parameters are anisotropic, and the averaging over m is mainly for display purposes; in the LES, the full m and n dependent parameters are used. The net dissipation matrix parameters, \mathbf{D}'_n , are shown as dashed lines in Fig. 2. The ‘barotropic’ diagonal element (D'_{11}) is negative at all wavenumbers while the ‘baroclinic’ (D'_{22}) diagonal element is positive at all wavenumbers. This is consistent with the phenomenology of quasigeostrophic two-layer turbulence [6]. The barotropic energy is cascaded towards lower wavenumbers while the baroclinic energy is cascaded towards higher wavenumbers for wavenumbers larger than the deformation scale. This explains the negative (diagonal) barotropic dissipation and positive (diagonal) baroclinic dissipation. The off-diagonal elements of \mathbf{D}'_n are also significant; the D'_{12} element in particular. The latter is negative at all scales; the D'_{21} element is mostly positive. Upon running the LES at T31, we find that the deterministic formulation (employ-

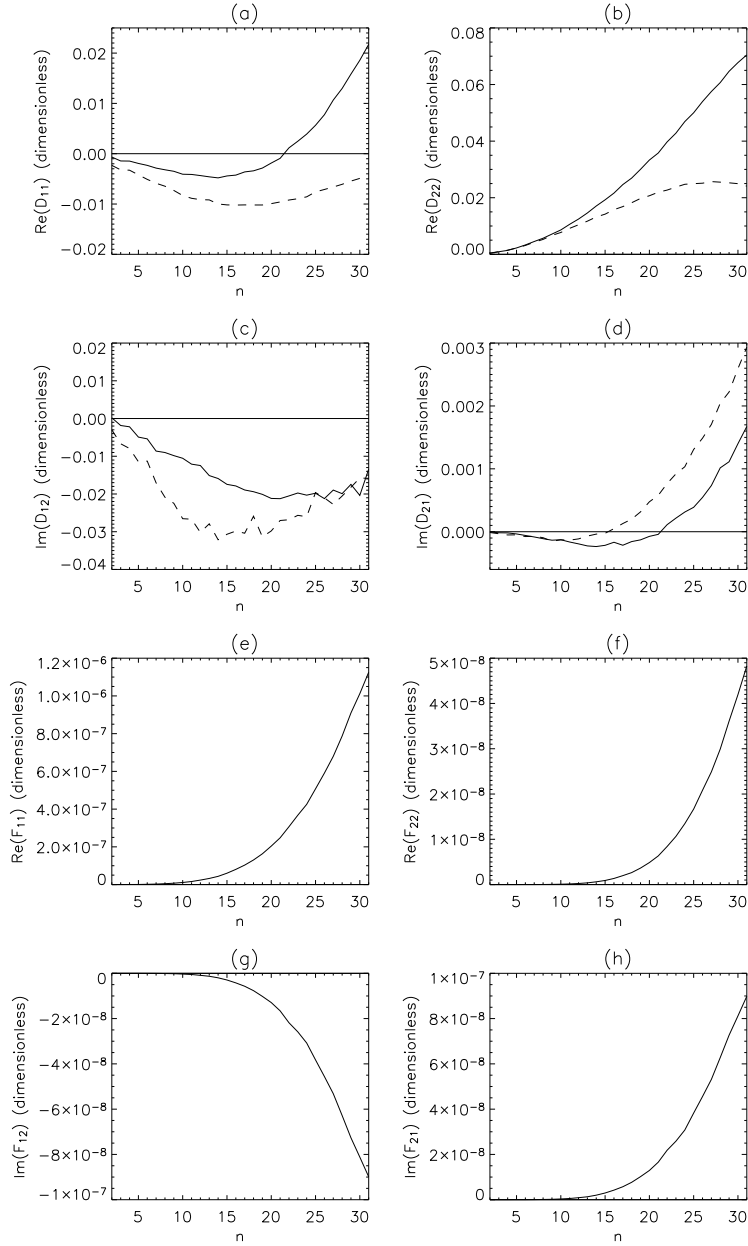


Figure 2: Eddy dissipation and backscatter covariance matrix coefficients: (a) $Re(D'_{11})$, (b) $Re(D'_{22})$, (c) $Im(D'_{12})$, (d) $Im(D'_{21})$, (e) $Re(F_{11})$, (f) $Re(F_{22})$, (g) $Im(F_{12})$, and (h) $Im(F_{21})$ as functions of total wavenumber (n) with $N_* = 31$. Stochastic parameterization (solid) and deterministic parameterization (dashed).

ing \mathbf{D}_n) is numerically unstable. It is likely that the instability is caused by the negative values of the diagonal barotropic elements.

For the stochastic parameterization, the matrix parameters \mathbf{D}'_d and \mathbf{F}' have been calculated using an integration time, τ , of 4 days; they are shown as solid lines in Fig. 2, after being averaged over the zonal wavenumber, m . The barotropic diagonal element of \mathbf{D}'_d rises to a positive cusp near the truncation scale, and is only slightly negative at low wavenumbers. The baroclinic diagonal element remains positive at all scales, rising to a cusp near the truncation scale. The off-diagonal elements are qualitatively similar to those of \mathbf{D}'_n , but are changed somewhat in terms of magnitude. The barotropic diagonal element of \mathbf{F}' rises to a cusp near the truncation scale; it is over an order of magnitude greater than the baroclinic diagonal element. The off-diagonal elements of \mathbf{F}' are complex conjugates, and are an order of magnitude less than F'_{11} (but greater than F'_{22}). The LES at T31 has been run with \mathbf{D}_d and \mathbf{F} , and the kinetic energy (Level 1) spectrum is shown in Fig. 3. The agreement between the LES at T31 and the higher resolution simulation is seen to be excellent.

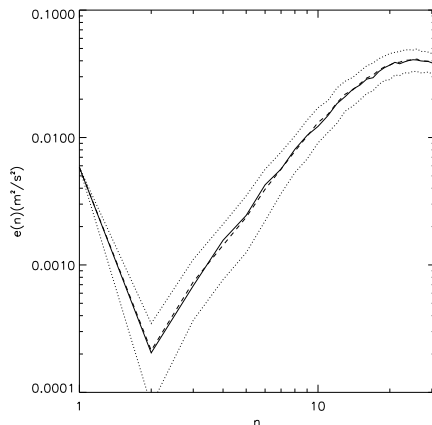


Figure 3: Energy spectra as functions of total wavenumber (n): kinetic energy for T31 LES (solid); T126 LES kinetic energy truncated back to T31 (dashed); and T31 LES kinetic energy plus and minus standard deviation (dotted).

Note that in these simulations we have set $\bar{\mathbf{f}} = 0$ as it was found to be sufficiently small. Our explanation for this is that the mean potential energy of the $(m, n) = (0, 1)$ mode is much larger than the transient energy [see Fig. 1(a)]; hence, the change in the mean field due to the conversion of potential

energy to kinetic energy is very small. This is not expected to be true in general. If the distribution of the mean field is more complex such that other zonal modes have mean components, then the change of potential energy is not expected to be negligible compared to the kinetic energy and $\bar{\mathbf{f}}$ cannot be neglected. This is demonstrated in the thesis of Zidikheri [8]. Additionally, in this study, we have set $\hat{\mathbf{x}} \rightarrow \mathbf{x}$ ($\hat{q}_{mn} \rightarrow q_{mn}$) in Eqs. 6 and 8 as only the $(m, n) = (0, 1)$ mode has a significant mean component (and does not contribute significantly to the *transient* subgrid flux).

5 Discussion and Conclusion

We can summarize the main result of this study by using a heuristic equation for the barotropic part of the LES:

$$\frac{\partial x}{\partial t} = \text{resolved terms} - Dx + f. \quad (17)$$

Here x is a resolved barotropic flow mode of wavenumber k , D is a scale-dependent subgrid eddy dissipation, and f is a scale-dependent subgrid eddy forcing comprising the random forcing and possibly the off-diagonal dissipation term. If $D < 0$, for some wavenumbers k , then those amplitudes will tend to grow. However, the non-linear terms will tend to limit the growth of the instability if there is an adequate sink at either the large or small scales. Hence, for example, if D is sufficiently positive near the truncation scale, then the simulation may well be stable. This is precisely the case for the T31 barotropic drain eddy dissipation calculated in this study. It was found to be slightly negative at the large scales, but had a positive cusp near the truncation scale, and was found to lead to a numerically stable LES. In contrast, we have found that if we try to work with the net dissipation and set the random part of f to zero, then the simulation becomes unstable. It is not hard to see why this might happen. The barotropic net dissipation is negative for all wavenumbers k in low resolution oceanic simulations; hence, there is not sufficient dissipation in the LES to control the growth caused by the negative dissipation term. With the stochastic formulation, D has a positive cusp, and furthermore, the white-noise forcing has the effect of de-correlating the flow in time, which helps to stabilize the system. The stochastic formulation also has the advantage of simulating the chaotic nature of the interaction between the resolved and subgrid scales in a more realistic fashion.

In conclusion, we state that the barotropic energy injection in low-resolution oceanic models is an important feature of the dynamics that is not

adequately captured by ocean circulation models at present. The stochastic methodology that we have presented has been shown to lead to stable net energy injecting simulations, which are in excellent agreement with higher resolution simulations. It is consistent with closure theories of turbulence, but employs DNSs. Therefore, it offers great promise in tackling the oceanic mesoscale eddy parameterization problem in more complex models as demonstrated in the thesis of Zidikheri [8].

References

- [1] J. R. Holton. *An Introduction to Dynamic Meteorology*. Academic Press, 1992.
- [2] Leith, C.E., Atmospheric predictability and two-Dimensional Turbulence, *J. Atmos. Sci.*, **28**, 1971, 145–161.
- [3] Kraichnan, R.H., Eddy viscosity in two and three Dimensions, *J. Atmos. Sci.*, **33**, 1976, 1521–1536.
- [4] Herring, J.R. Subgrid scale modeling – An introduction and overview. F. Durst, B. Launder, F. Schmidt, J. Whitelaw, editors, *Turbulent Shear Flows 1*. Springer-Verlag, 1979.
- [5] Frederiksen, J.S., and A.G. Davies, Eddy viscosity and stochastic backscatter parameterizations on the sphere for atmospheric circulation models, *J. Atmos. Sci.*, **54**, 1997, 2475–2492.
- [6] Salmon, R., Two-layer quasi-geostrophic turbulence in a simple special case, *Geophys. Astrophys. Fluid Dynamics*, **10**, 1978, 25–52.
- [7] Frederiksen, J.S. and S.M. Kepert, Dynamical subgrid-scale parameterizations from direct numerical simulations, *J. Atmos. Sci.*, **63**, 2006, 3006–3019.
- [8] Zidikheri, M.J. *Dynamical Subgrid-scale parameterizations for Quasi-geostrophic Flows using Direct Numerical Simulations*, PhD Thesis, The Australian National University, 2008.
- [9] Bourke, W., An efficient, one-Level, primitive-equation spectral model, *Mon. Weath. Rev.*, **100**, 1972, 683–689.